DOI: 10.1002/ejic.201100151

Non-Aqueous Preparation of High-Crystallinity Hierarchical TiO_2 Hollow Spheres with Excellent Photocatalytic Efficiency

Xujie Lü,[a] Shangjun Ding,[a] Yian Xie,[a] and Fuqiang Huang*[a,b]

Keywords: Nanostructures / Crystal growth / Titanium / Synthetic methods / Photolysis

High-crystallinity hierarchical anatase TiO_2 hollow spheres were prepared by a high-temperature (350 °C) and non-aqueous solvothermal method in the absence of water, templates, or additives. The hollow structures were assembled from highly crystallized TiO_2 nanoparticles and exhibit superior photocatalytic properties relative to those of Degussa P25 TiO_2 under irradiation with UV light. The influence of reaction temperature on the crystallinity, morphology, crystallite shape and size, band gap, specific surface area, and pore size distribution of TiO_2 has been studied in detail. It is evident that reaction temperature is the most important factor to increase the crystallinity of TiO_2 in order to improve its charge transfer and transport properties, which are important in photocatalysis.

Introduction

Titanium dioxide (TiO_2) has been widely used in photocatalysis, dye-sensitized solar cells (DSCs), Li batteries, transparent conductors, gas sensors, and so on.[1] Its physicochemical properties are strongly dependent on its phase composition, crystallinity, crystal size, specific surface area, and porosity. Controllable preparation of well-crystallized nanostructured anatase (TiO_2) is highly desired for many applications. The perfectly ordered lattice (high crystallinity) of TiO_2 can reduce the formation of electron traps and facilitate electron transfer,[2] and an assembled hierarchical nanostructure can provide a particular morphology, microsize, and pore-size distribution to further meet specific device requirements.[3] The traditional two-step route to high-crystallinity nanostructured TiO_2 is calcining low-crystallinity or amorphous TiO_2 nanostructures by using organic additives (surfactants, templates),[4] but the high-temperature treatment can cause particle agglomeration, pore collapse, severe decline in surface area, and undesired phase transformation. Solvothermal processes have been demonstrated to be one of best preparation methods to produce well-crystallized TiO_2 particles with different morphologies.[5] However, most titanium precursors are extremely sensitive to moisture, and some organic additives may be required.[6] The reaction temperature is usually below 250 °C due to the softening temperature of Teflon containers. Therefore, it was greatly preferred to explore a higher-temperature, non-aqueous, additive-free solvothermal method to synthesize high-crystallinity TiO_2. In addition, for the application of TiO_2 in photocatalysis, although some samples with higher photocatalytic activity than P25, such as TiO_2 nanocrystals with a high-energy surface of (001)[7] and TiO_2 ultrafine nanopowders with large surface area,[8] have been reported, preparing photocatalysts with a performance better than P25 is still not easy to be achieved by a very simple synthetic route.

Herein, we report highly crystallized TiO_2 nanoparticles and their assembled mesoporous hollow structures prepared by a simple non-aqueous solvothermal route at 350 °C. The specific morphology of these nanoparticles can be tuned by altering the volume ratio of titanium *n*-butoxide (TNB) and ethanol (EtOH). The reaction temperature significantly affected the crystallinity of TiO_2 nanoparticles and their assembled morphology and pore structures. The TiO_2 nanoparticles prepared at 350 °C have better photocatalytic efficiency than that of Degussa P25, because of their high crystallinity. The assembled microscale hollow spheres also exhibit equivalent photoactivity but are easier to be recycled relatibe to P25. These high-crystallinity TiO_2 particles are expected to possess excellent electron transport ability in DSCs.

Results and Discussion

Effect of Reaction Temperature

No water and organic additives were introduced into the reaction except the reagents EtOH and TNB. TiO_2 powders were only observed starting at 250 °C. The fixed volume ratio of TNB/EtOH = 1:1 was used to investigate the influ-

[a] CAS Key Laboratory of Materials for Energy Conversion, Shanghai Institute of Ceramics, Chinese Academy of Sciences, Shanghai 200050, P. R. China
Fax: +86-21-5241-6360
E-mail: huangfq@mail.sic.ac.cn
[b] College of Chemistry & Molecular Engineering, Peking University,
Beijing 100871, P. R. China
Supporting information for this article is available on the WWW under http://dx.doi.org/10.1002/ejic.201100151.

ence of reaction temperature, and three samples, denoted as S250, S300, and S350, were prepared at 250, 300, and 350 °C, respectively. All the XRD patterns of the as-prepared powders can be assigned to the anatase phase of TiO_2 (JCPDS No. 21–1272), as shown in Figure 1a. As the reaction temperature increased, the significant improvement of the crystallinity was evident from the higher diffraction peak intensity and the smaller full width at half maximum (FWHM). According to the Scherrer equation based on the main peak (101), the respective average crystallite sizes were calculated to be 8.4 (S250), 19.1 (S300), and 30.2 nm (S350), as shown in Figure 1b. This result demonstrated that crystal growth could be greatly promoted by high reaction temperature. The approximate lattice strain of these samples, calculated by using the Williams and Hall equation (see Table S1 and Figure S1 in the Supporting Information), decreased obviously with increasing reaction temperature (Figure 1b), which also indicates the significant improvement of the crystallinity. In order to compare the new crystals with those of Degussa P25 powder, the XRD pattern, crystallite size, and lattice strain are illustrated in Figure 1. The sample synthesized at the highest temperature (S350) evidently exhibits better crystallinity and larger crystallite size than P25, while S300 is similar to P25.

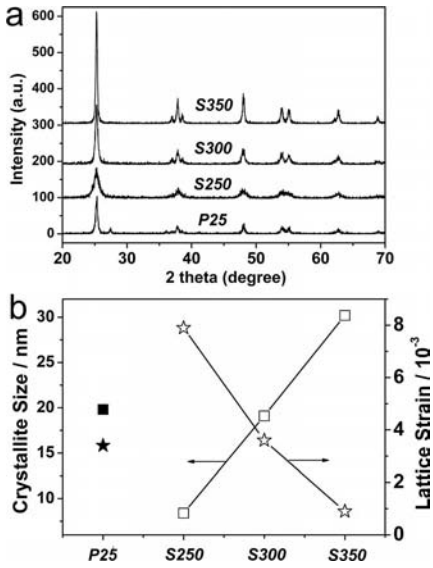

Figure 1. (a) XRD diffraction patterns of the TiO_2 samples prepared at different temperatures. (b) The corresponding crystallite size and lattice strain variation with reaction temperature calculated by the Scherrer and Williams–Hall equations.

From the UV/Vis diffuse reflectance spectra of these samples, a plot of the modified Kubelka–Munk function $[F(R) = (1 - 2R)^2/2R = \alpha/S]$[9] versus the energy of the exciting light is shown in Figure S2 to obtain more precise optical band gaps. With increasing reaction temperature, the onset of the absorption shifts to longer wavelength slightly, and the band gap decreases from 3.21 to 3.16 eV in accordance with the quantum size effect. The commercial P25 has a narrower band gap, 3.07 eV, for the anatase phase and 2.98 eV for the rutile phase.

The morphologies of the as-prepared samples vary with reaction temperature (Figure 2). A large amount of the particles are spheres in the as-prepared samples. But the TiO_2 spheres in S250 are smaller and smoother than the others, and the proportion of spheres in S300 is lower. In S350, rougher nanoparticle-assembled microspheres with larger diameters are observed, and some broken spheres reveal a hollow interior (Figure 3). The selected high-resolution images clearly show a mesoporous structure. In order to investigate the pore structure evolution of these samples, nitrogen adsorption/desorption isotherms were measured and the pore size distributions were calculated by the Barrett–Joyner–Halenda (BJH) method (Figure 4). The pore size increased from 4.2 (S250) to 30.5 nm (S350), but the BET surface area decreased from 172.85 (S250) to 28.18 $m^2 g^{-1}$ (S350), as shown in Table 1.

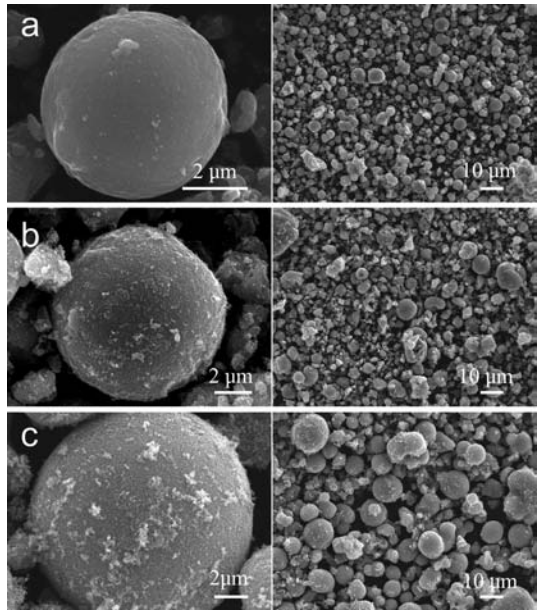

Figure 2. SEM images of the as-prepared TiO_2 samples: (a) S250, (b) S300, (c) S350.

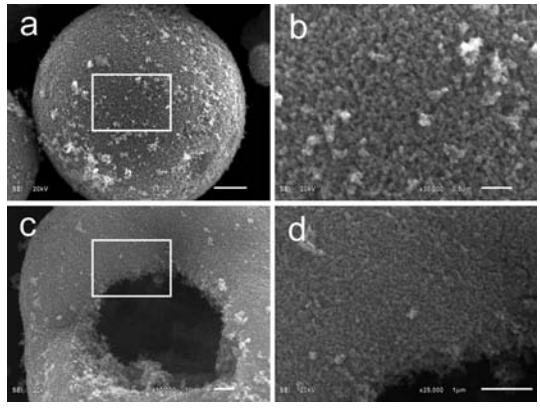

Figure 3. SEM images of the S350 TiO_2 sample, (a) a whole sphere, (b) magnified image of the selected part in (a), (c) a broken hollow sphere, (d) magnified image of the selected part in (c).

The nano-TiO_2 particles were dispersed from microspheres by using high-power supersonic treatment and in-

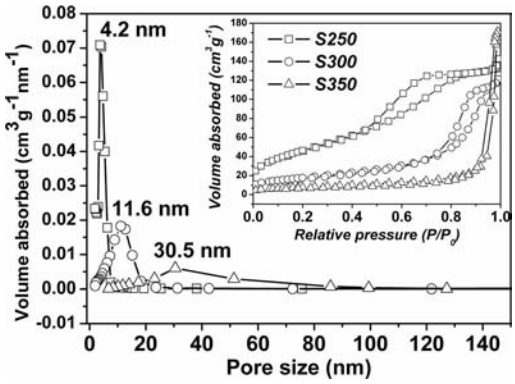

Figure 4. Nitrogen adsorption/desorption isotherm (inset) and the corresponding pore size distribution of the TiO_2 samples prepared at different temperatures.

Table 1. Characteristics of different TiO_2 samples.

Sample	Crystal size [nm]	Specific surface area [m^2g^{-1}]	Pore volume [cm^3g^{-1}]	Pore size [nm]
S250	8.4	172.85	0.229	4.2
S300	19.1	64.41	0.195	11.6
S350	30.2	28.18	0.266	30.5
P25[a]	21.1	56	0.25	17.5

[a] This refers to the characterization of Degussa P25 in ref.[10]

vestigated by TEM (Figure 5). The nanoparticles of these three samples have different shapes and sizes as well as different crystallinity. Irregular crystallites were observed in S250 (Figure 5a), spindle-shape particles in S300 (Figure 5b), and largest and polygon-like shapes in S350 (Figure 5c). The HRTEM and SAED images show the significant improvement of crystallinity of the nanoparticles with increasing reaction temperature, and the reaction temperature of 350 °C may be the optimal condition to synthesize well-crystallized nano-TiO_2.

Effect of Precursor Concentration

The morphology of S350 can be tuned by adjusting the volume ratio of TNB and EtOH, as shown in Figure 6. Assembled hierarchical nanoparticle spheres can only be obtained when the volume ratio EtOH/TNB is in an appropriate range. The porous structure is obvious at EtOH/TNB = 3:1 and 1:1 from the SEM image. At higher ratios (e.g., 10:1) the nanoparticles diminish in size and the spherical surfaces are smoother. At EtOH/TNB < 1:1, the hollow spheres shrink and collapse to irregular shapes. Under extreme conditions, pure TNB decomposed at 350 °C to form well-crystallized TiO_2 nanoparticles, but the spherical shapes were not retained. It is evident that the molar ratio of EtOH/TNB plays an important role on the formation of hollow spheres. The crystallinity of these as-prepared sam-

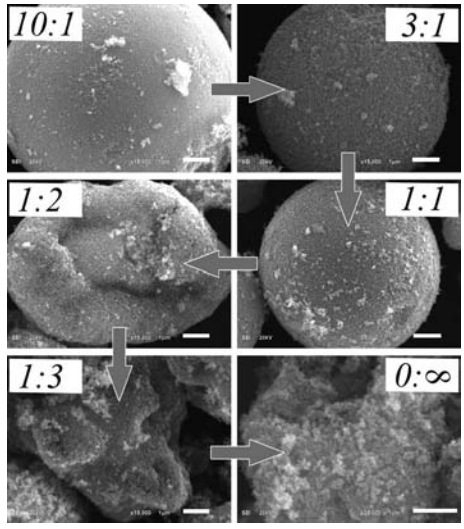

Figure 6. The SEM morphology variation of the TiO_2 prepared at 350 °C with different volume ratios of EtOH/TNB (scale bar: 1 μm).

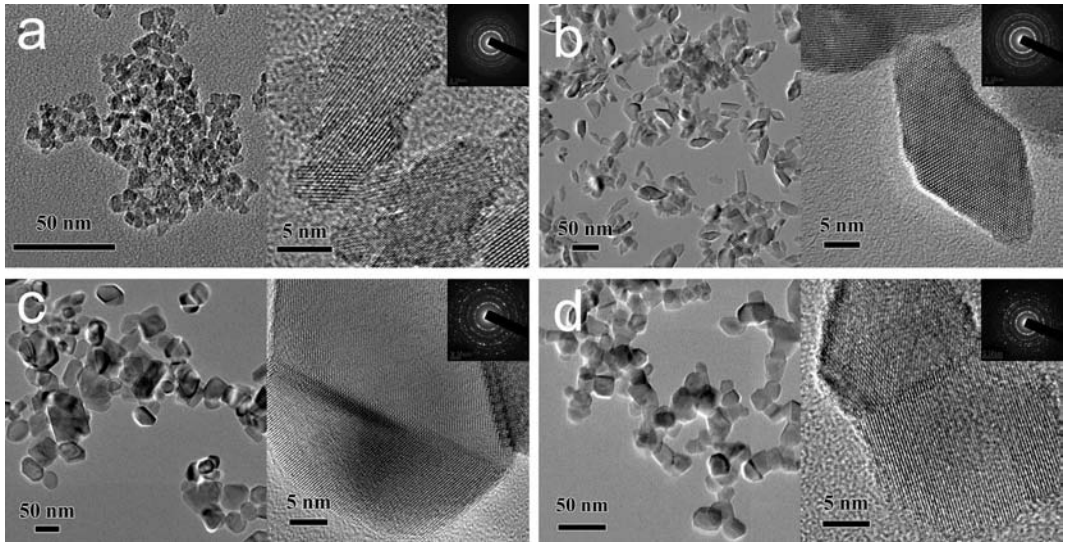

Figure 5. TEM, HRTEM, and SAED patterns of the TiO_2 nanoparticles prepared at different temperatures: (a) S250, (b) S300, (c) S350, (d) P25.

ples was studied by XRD (Figure S3), and particularly low TNB concentration (e.g. 10:1) was found to result in smaller crystallite size and poorer crystallinity.

Photocatalytic Performance

Figure 7 depicts the results of the photocatalytic degradation of methyl orange (MO) over the different TiO_2 samples. The photocatalytic efficiency decreases gradually in the order S350 > S300 > S250, in agreement with the decreasing crystallinity. Specific surface area and crystallinity are the primary factors to influence the photocatalytic activity of TiO_2 in this case. With increasing reaction temperature, the notable improvement of crystallinity compensates the shortcomings of decreasing specific surface area, as listed in Table 1. So the photocatalytic efficiency of the S350 is comparable to that of P25, while S250 exhibits inferior performance despite its high specific surface area.

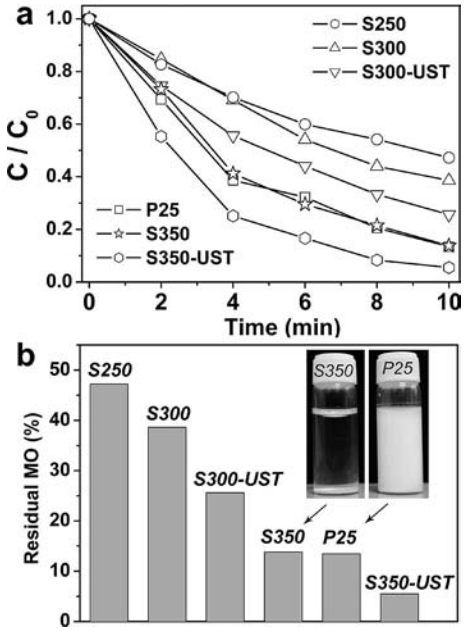

Figure 7. (a) Photocatalytic degradation of methyl orange (MO) by different TiO_2 samples, (b) comparison of photocatalytic activities of different TiO_2 samples under 10 min UV-light irradiation and the photograph (inset) of S350 and P25 suspensions after precipitation for 30 min.

In order to evaluate the photocatalytic reactivity of the nanoparticles constituting the spheres, the nanoparticles in the S300 and S350 microspheres were dissociated by high-power ultrasonic treatment, and the obtained samples were denoted S300-UST and S350-UST, respectively. S350-UST was found to possess superior photocatalytic efficiency over P25 and S350. S300-UST has crystallinity, crystallite size, and specific surface area similar to those of P25, but its photocatalytic efficiency is lower than that of P25, which may be due to the rutile–anatase nanocomposite effect of P25. However, the microscale nanoparticle-assembled photocatalysts S350 can easily be recycled (inset of Figure 7b), which is also an advantage over P25 in addition to the comparable photocatalysis.

Possible Growth Mechanism

In the present method, the water supply for hydrolysis was chemically introduced, which is appropriate for the high moisture sensibility of the titanium alkoxide precursor. The occurrence of etherifying reactions to generate water was proven by GC-MAS studies (Figure S4). Three typical ethers (ethyl ether, ethyl *n*-butyl ether, and dibutyl ether) were detected, and they were probably generated by the reactions shown in Equations (1), (2), (3), and (4). The different reaction temperatures may lead to different reaction types and growth mechanisms. At low temperature (250 °C), the water from esterification can hydrolyze TNB to TiO_2 gradually according to Equations (1)–(5). As a result of the limited amount of water, the obtained TiO_2 crystallites are small, and they assemble to microspheres with nanosized pores. Higher reaction temperatures allow the production of sufficient water for hydrolysis to facilitate large preferentially shaped nanocrystal growth. Pure TNB can decompose to TiO_2 nanoparticles above 350 °C and produce some gas. The gas may be 1-butyne [Equation (6)] according to GC-MAS measurements, which can serve as bubble templates for the growth of hollow TiO_2 structures. Large and well-crystallized TiO_2 nanocrystals were formed at 350 °C and assembled on the bubble surface to create the hierarchical hollow structure. The possible growth mechanism at different temperatures is shown in Figure 8.

$$EtOH + EtOH \rightarrow Et–O–Et + H_2O \quad (1)$$

$$Ti(BuO)_4 + H_2O \rightarrow Ti(BuO)_3OH + BuOH \quad (2)$$

$$BuOH + EtOH \rightarrow Bu–O–Et + H_2O \quad (3)$$

$$2BuOH \rightarrow Bu–O–Bu + H_2O \quad (4)$$

$$Ti(BuO)_3OH + Ti(BuO)_4 \rightarrow (BuO)_3\mathbf{Ti–O–Ti}(BuO)_3 + BuOH \quad (5)$$

$$Ti(BuO)_4 \rightarrow TiO_2 + CH_3CH_2CH{\equiv}CH \uparrow \quad (6)$$

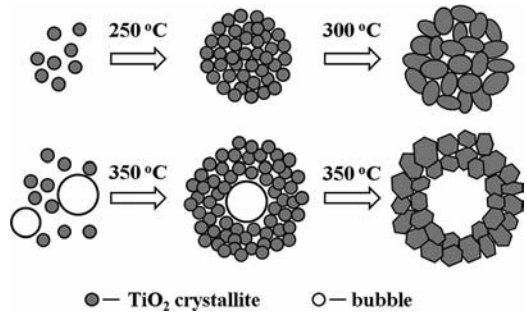

Figure 8. Growth mechanism of TiO_2 spheres at different temperatures.

Conclusions

In this study, a facile method was proposed to prepare high-crystallinity TiO_2 spheres with higher photocatalytic

activity than that of Degussa P25 by a high-temperature (350 °C) and non-aqueous solvothermal route. The water for hydrolysis is self-provided in the reaction system. In addition to the superior photocatalytic performance, the as-prepared TiO_2 samples are easy to handle and to recover (for example, by sedimentation) in practical applications.

Experimental Section

Synthesis: The chemicals $Ti(OBu)_4$ (TNB, analytically pure), and ethanol (EtOH, analytically pure) were used without further purification. In a typical procedure, the mixed solution of TNB and EtOH was prepared by slowly adding TNB to EtOH with a certain volume ratio. After stirring for 30 min, the mixture was transferred into a stainless steel autoclave (10 mL capacity, 70% filling) for solvothermal reaction at a desired temperature for 4 h. Followed by cooling gradually to room temperature, the precipitate was collected by filtering, washing with anhydrous ethanol for three times, and drying at 80 °C overnight.

Characterization: The analysis of the crystalline structure and phase identification of the samples were performed by X-ray diffraction (XRD Bruker D8 ADVANCE) with a monochromatized source of Cu-K_α1 radiation (λ = 0.15405 nm) at 1.6 kW (40 KV, 40 mA). A JEOL JSM-6510 scanning electron microscope (SEM) was used to investigate the morphologies of the samples. Field-emission transmission electron microscopy (TEM) as well as high-resolution transmission electron microscopy (HRTEM) images was collected by using a JEOL JEM 2100F microscope working at 200 kV. The optical absorption characteristics of the powders were determined by UV/Vis diffuse reflectance spectroscopy (DRS) on a spectrophotometer (Hitachi U4100) equipped with an integrating sphere. Nitrogen adsorption/desorption isotherms at 77 K were measured with a Micromeritics Tristar 3000 system. The pore size distributions were calculated from desorption branches of isotherms by the Barrett–Joyner–Halenda (BJH) method. The species of organic reaction products were characterized with a combination of gas chromatography and mass spectrometry (GC–MS) (Agilent, 6890N/5973N). The photocatalytic activity of the samples was evaluated by the photocatalytic degradation of a model pollutant, methyl orange (MO), under UV light (generated by a 500 W high-pressure mercury lamp). The photocatalyst (ca. 100 mg) was added into MO solution (200 mL, 10 mg L^{-1}). After being stirred in the dark for 30 min to reach the adsorption/desorption equilibrium, the suspension was exposed to light irradiation whilst stirring. The concentrations of MO were monitored by checking the absorbance at 464 nm during the degradation process with a Hitachi U-3010 UV/Vis spectrophotometer.

Supporting Information (see footnote on the first page of this article): The method to evaluate lattice strain by using the Williams and Hall Equation, XRD patterns of the TiO_2 samples prepared at different volume ratios of EtOH/TNB, and GC-MAS spectrum characterization of the reaction solution at 350 °C.

Acknowledgments

This work is financially supported by the National 973 Program of China (grant numbers 2009CB939903 and 2007CB936704), the National Natural Science Foundation of China (grant numbers 50772123 and 50821004), and the Science and Technology Commission of Shanghai (grant numbers 0752 nm016, 0952 nm06500, and 08JC1420200).

[1] a) J. J. Wu, X. J. Lü, L. L. Zhang, F. Q. Huang, F. F. Xu, *Eur. J. Inorg. Chem.* **2009**, *19*, 2789–2795; b) M. Li, Z. L. Hong, Y. N. Fang, F. Q. Huang, *Mater. Res. Bull.* **2008**, *43*, 2179–2186; c) X. J. Lü, J. J. Wu, D. W. Zhang, L. L. Zhang, F. Q. Huang, F. F. Xu, S. M. Huang, *Adv. Funct. Mater.* **2010**, *3*, 509–515; d) X. J. Lü, F. Q. Huang, X. L. Mou, Y. M. Wang, F. F. Xu, *Adv. Mater.* **2010**, *22*, 3719–3722; e) H. X. Li, Z. F. Bian, J. Zhu, D. Q. Zhang, G. S. Li, Y. N. Huo, H. Li, Y. F. Lu, *J. Am. Chem. Soc.* **2007**, *129*, 8406–8407; f) S. C. Yang, D. J. Yang, J. Kim, J. M. Hong, H. G. Kim, I. D. Kim, H. Lee, *Adv. Mater.* **2008**, *20*, 1059–1064; g) D. Kim, A. Ghicov, S. P. Albu, P. Schmuki, *J. Am. Chem. Soc.* **2008**, *130*, 16454–16455; h) S. W. Kim, T. H. Han, J. Kim, H. Gwon, H. S. Moon, S. W. Kang, S. O. Kim, K. Kang, *ACS Nano* **2009**, *3*, 1085–1090; i) S. X. Zhang, S. Dhar, W. Yu, H. Xu, S. B. Ogale, T. Venkatesan, *Appl. Phys. Lett.* **2007**, *11*, 112113–112115; j) S. Joo, I. Muto, N. Hara, *J. Electrochem. Soc.* **2010**, *157*, 221–226.

[2] a) J. Ovenstone, *J. Mater. Sci.* **2001**, *36*, 1325–1329; b) Y. Qu, W. Zhou, K. Pan, C. G. Tian, Z. Y. Ren, Y. Z. Dong, H. G. Fu, *Phys. Chem. Chem. Phys.* **2010**, *12*, 9205–9212.

[3] a) D. S. Kim, S. Y. Kwak, *Appl. Catal. A* **2007**, *323*, 110–118; b) B. Liu, E. S. Aydil, *J. Am. Chem. Soc.* **2009**, *131*, 3985–3990.

[4] a) D. T. On, *Langmuir* **1999**, *15*, 8561–8564; b) S. H. Elder, Y. Gao, X. Li, J. Liu, D. E. McCready, C. F. Windisch Jr., *Chem. Mater.* **1998**, *10*, 3140–3145.

[5] a) G. H. Tian, H. G. Fu, L. Q. Jing, B. F. Xin, K. Pan, *J. Phys. Chem. C* **2008**, *112*, 3083–3089; b) L. Zhao, X. F. Chen, X. C. Wang, Y. J. Zhang, W. Wei, Y. H. Sun, *Adv. Mater.* **2010**, *22*, 3317–3321; c) X. L. Li, Q. Peng, J. X. Yi, X. Wang, Y. D. Li, *Chem. Eur. J.* **2006**, *12*, 2383–2391.

[6] a) K. Kanie, T. Sugimoto, *Chem. Commun.* **2004**, *14*, 1584–1585; b) D. Jiang, Y. Xu, B. Hou, D. Wu, Y. H. Sun, *Eur. J. Inorg. Chem.* **2008**, *8*, 1236–1240.

[7] a) H. G. Yang, G. Liu, S. Z. Qiao, C. H. Sun, Y. G. Jin, S. C. Smith, J. Zou, H. M. Cheng, G. Q. Lu, *J. Am. Chem. Soc.* **2009**, *131*, 4078–4083; b) H. G. Yang, C. H. Sun, S. Z. Qiao, J. Zou, G. Liu, S. C. Smith, H. M. Cheng, G. Q. Lu, *Nature* **2008**, *453*, 638–641.

[8] S. Chin, E. Park, M. Kim, J. Jeong, G.-N. Bae, J. Jurng, *Powder Technol.* **2011**, *206*, 306–311.

[9] J. Klaas, G. Schulz-Ekloff, N. I. Jaeger, *J. Phys. Chem. B* **1997**, *101*, 1305–1311.

[10] K. J. A. Raj, B. Viswanathan, *Ind. J. Chem. A* **2009**, *48*, 1378–1382.

Received: February 15, 2011
Published Online: May 17, 2011

